

structure, spectra of which were fully consistent with the natural isolate.

The mechanism of the conjunctive coupling reaction is the subject of ongoing investigations, although the substrate scope (Figs. 2 and 3) gives clues about the process. The observation that electron-deficient arenes are less prone to migration is consistent with the mechanistic hypothesis put forward in Fig. 1E. According to this hypothesis, formation of **IV** would likely be stereochemistry determining, and, in line with this prediction, the selectivity of the reaction depends not only on the ligand framework but also on the organoboronic ester ligand (pinacol versus *neo*-pentylglycol), the migrating group, and the electrophile. In addition to these observations, one preliminary experiment sheds important light on the nature of the metal-induced metallate rearrangement that appears to underlie the conjunctive coupling process. As depicted in Fig. 4B, when the reacting ate complex was constructed from stereochemically defined deuterium-labeled vinylolithium (**27**) and phenylB(pin), the (*1R,2R*) stereoisomer of the conjunctive coupling product was formed in >20:1 diastereoselection (82:18 er). Although other interpretations are possible, should the mechanism be in line with that proposed in Fig. 1E and reductive elimination occur with retention of configuration at carbon (a reasonable assumption), the observed stereochemical outcome in Fig. 4B is consistent with anti-migration of the arene group to a Pd-olefin complex (Fig. 1D). Such an outcome is reminiscent of nucleometallation reactions that do not involve preassociation of the migrating group and the metal center (**28**).

We anticipate that many other transition metal-catalyzed reactions might also be reengineered to incorporate metal-induced metallate rearrangements, thereby providing distinct strategies for catalytic enantioselective synthesis.

## REFERENCES AND NOTES

- D. G. Hall, Ed., *Boronic Acids* (Wiley-VCH, Weinheim, Germany, 2011).
- N. Miyaura, K. Yamada, A. Suzuki, *Tetrahedron Lett.* **20**, 3437–3440 (1979).
- N. Miyaura, A. Suzuki, *Chem. Rev.* **95**, 2457–2483 (1995).
- T. Jia et al., *J. Am. Chem. Soc.* **137**, 13760–13763 (2015).
- W. Su et al., *Angew. Chem. Int. Ed.* **54**, 12957–12961 (2015).
- E.-I. Negishi, *Org. React.* **33**, 1–246 (1985).
- V. K. Aggarwal, G. Y. Fang, X. Ginesta, D. M. Howells, M. Zaja, *Pure Appl. Chem.* **78**, 215–229 (2006).
- M. M. Midland, A. R. Zolopa, R. L. Halterman, *J. Am. Chem. Soc.* **101**, 248–249 (1979).
- A. Suzuki, *Top. Curr. Chem.* **112**, 67–115 (1983).
- P. M. Draper, T. H. Chan, D. N. Harpp, *Tetrahedron Lett.* **11**, 1687–1688 (1970).
- S. P. Thomas, R. M. French, V. Jheengut, V. K. Aggarwal, *Chem. Rec.* **9**, 24–39 (2009).
- D. Leonori, V. K. Aggarwal, *Top. Organomet. Chem.* **49**, 271–295 (2015).
- P. K. Jadhav, H.-W. Man, *J. Am. Chem. Soc.* **119**, 846–847 (1997).
- A. Suzuki et al., *J. Am. Chem. Soc.* **95**, 3080–3081 (1973).
- For lead references, see (29).
- G. Zweifel, H. Arzoumanian, C. C. Whitney, *J. Am. Chem. Soc.* **89**, 3652–3653 (1967).
- N. Ishida, Y. Shimamoto, M. Murakami, *Org. Lett.* **11**, 5434–5437 (2009).
- J. S. Nakhla, J. W. Kampf, J. P. Wolfe, *J. Am. Chem. Soc.* **128**, 2893–2901 (2006).
- D. Bruyère, D. Bouyssi, G. Balme, *Tetrahedron* **60**, 4007–4017 (2004).

- G. Berionni, A. I. Leonov, P. Mayer, A. R. Ofial, H. Mayr, *Angew. Chem. Int. Ed.* **54**, 2780–2783 (2015).
- K. Feeney, G. Berionni, H. Mayr, V. K. Aggarwal, *Org. Lett.* **17**, 2614–2617 (2015).
- A. Togni et al., *J. Am. Chem. Soc.* **116**, 4062–4066 (1994).
- J. J. Almerna Perea, M. Lotz, P. Knochel, *Tetrahedron Asymmetry* **10**, 375–384 (1999).
- D. Seyferth, M. A. Weiner, *J. Am. Chem. Soc.* **83**, 3583–3586 (1961).
- G. R. Pettit, G. M. Cragg, D. L. Herald, J. M. Schmidt, P. Lohavanijaya, *Can. J. Chem.* **60**, 1374–1376 (1982).
- R. Singh, H. Kaur, *Synthesis* **2009**, 2471–2491 (2009).
- R. P. Hughes, H. A. Trujillo, J. W. Egan Jr., A. L. Rheingold, *J. Am. Chem. Soc.* **122**, 2261–2271 (2000).
- R. I. McDonald, G. Liu, S. S. Stahl, *Chem. Rev.* **111**, 2981–3019 (2011).
- A. Bottoni, M. Lombardo, A. Neri, C. Trombini, *J. Org. Chem.* **68**, 3397–3405 (2003).

## ACKNOWLEDGMENTS

Experimental data are available in the associated Supplementary Materials. This research was supported in part by the NIH, National Institute of General Medical Sciences (GM 64451), and by Boston College. Metrical parameters for the crystal structure of compound **1** are available free of charge from the Cambridge Crystallographic Data Centre under accession number CCDC 1437520.

## SUPPLEMENTARY MATERIALS

www.sciencemag.org/content/351/6268/70/suppl/DC1  
Materials and Methods  
Tables S1 to S7  
References (30–57)

12 October 2015; accepted 18 November 2015  
10.1126/science.aad6080

## MICROBIAL ENGINEERING

# Self-photosensitization of nonphotosynthetic bacteria for solar-to-chemical production

Kelsey K. Sakimoto,<sup>1,2</sup> Andrew Barnabas Wong,<sup>1,2</sup> Peidong Yang<sup>1,2,3,4,\*</sup>

Improving natural photosynthesis can enable the sustainable production of chemicals. However, neither purely artificial nor purely biological approaches seem poised to realize the potential of solar-to-chemical synthesis. We developed a hybrid approach, whereby we combined the highly efficient light harvesting of inorganic semiconductors with the high specificity, low cost, and self-replication and -repair of biocatalysts. We induced the self-photosensitization of a nonphotosynthetic bacterium, *Moorella thermoacetica*, with cadmium sulfide nanoparticles, enabling the photosynthesis of acetic acid from carbon dioxide. Biologically precipitated cadmium sulfide nanoparticles served as the light harvester to sustain cellular metabolism. This self-augmented biological system selectively produced acetic acid continuously over several days of light-dark cycles at relatively high quantum yields, demonstrating a self-replicating route toward solar-to-chemical carbon dioxide reduction.

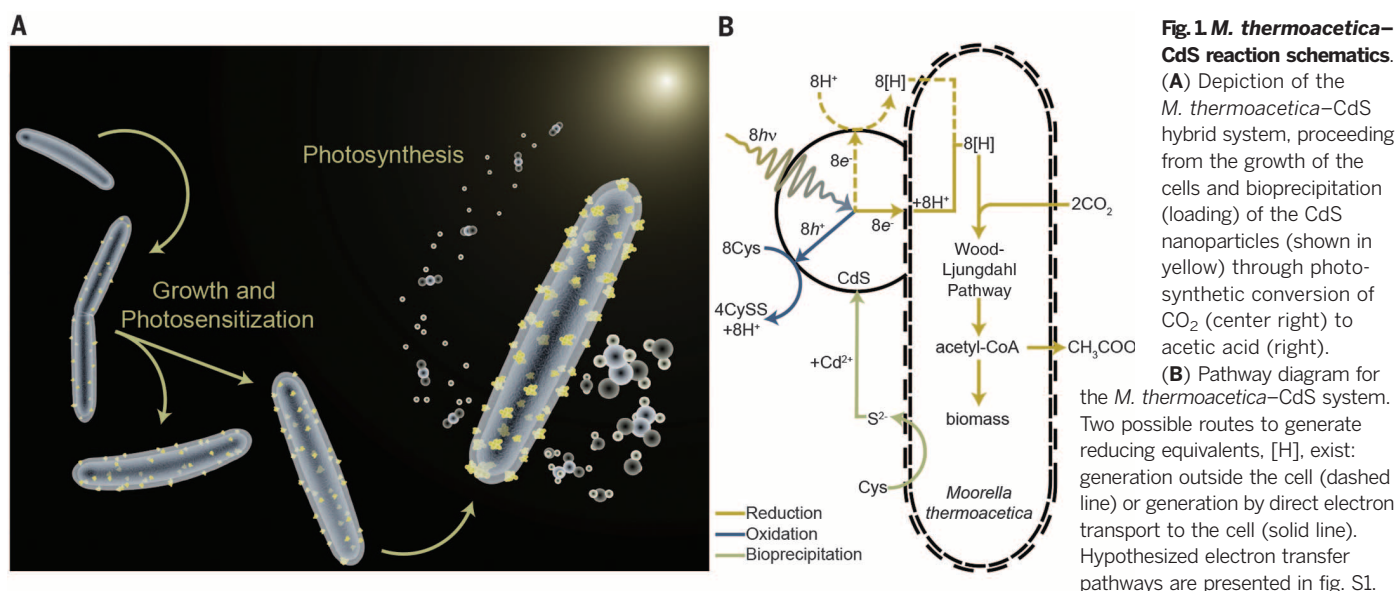
The necessity of improving the natural mechanisms of solar energy capture for sustainable chemical production (*1*) has motivated the development of photoelectrochemical devices based on inorganic solid-state materials (*2*). Although solid-state semiconductor light absorbers often exceed biological light harvesting in efficiency (*3*), the transduction of photoexcited electrons into chemical bonds (particularly toward multicarbon compounds from CO<sub>2</sub>) remains challenging with abiotic catalysts (*4, 5*). Such catalysts struggle to compete with the high-specificity, low-cost material requirements and the self-replicating, self-repairing properties of biological CO<sub>2</sub> fixation (*6*). Thus, a viable solution must combine the best of both worlds: the light-harvesting capabilities of semiconductors with the catalytic power of biology.

Several inorganic-biological hybrid systems have been devised: semiconductor nanoparticles with hydrogenases to produce biohydrogen (*7*), long wavelength-absorbing nanomaterials to improve the photosynthetic efficiency of plants (*8*), and whole cells with photoelectrodes for CO<sub>2</sub> fixation (*9, 10*). Whole-cell microorganisms are favored to facilitate the multistep process of CO<sub>2</sub> fixation and can self-replicate and self-repair (*11*). Furthermore, bacteria termed “electrotrophs” can undergo direct electron transfer from an electrode (*12*). However, traditional chemical synthesis of the semiconductor component often requires high-purity reagents, high temperatures, and complex microfabrication techniques. Additionally, the integration of such foreign materials with biotic systems is nontrivial (*13*). Many reports have shown that some microorganisms induce the precipitation of nanoparticles (*14*), producing an inherently biocompatible nanomaterial under mild conditions.

Although photosynthetic organisms can precipitate semiconductor nanoparticles, their metabolic pathways are arguably less desirable than those of their nonphotosynthetic counterparts. Although gene modification of phototrophs has

<sup>1</sup>Department of Chemistry, University of California–Berkeley, Berkeley, CA 94720, USA. <sup>2</sup>Materials Sciences Division, Lawrence Berkeley National Laboratory, Berkeley, CA 94720, USA. <sup>3</sup>Department of Materials Science and Engineering, University of California–Berkeley, Berkeley, CA 94720, USA. <sup>4</sup>Kavli Energy NanoSciences Institute, Berkeley, CA 94720, USA.

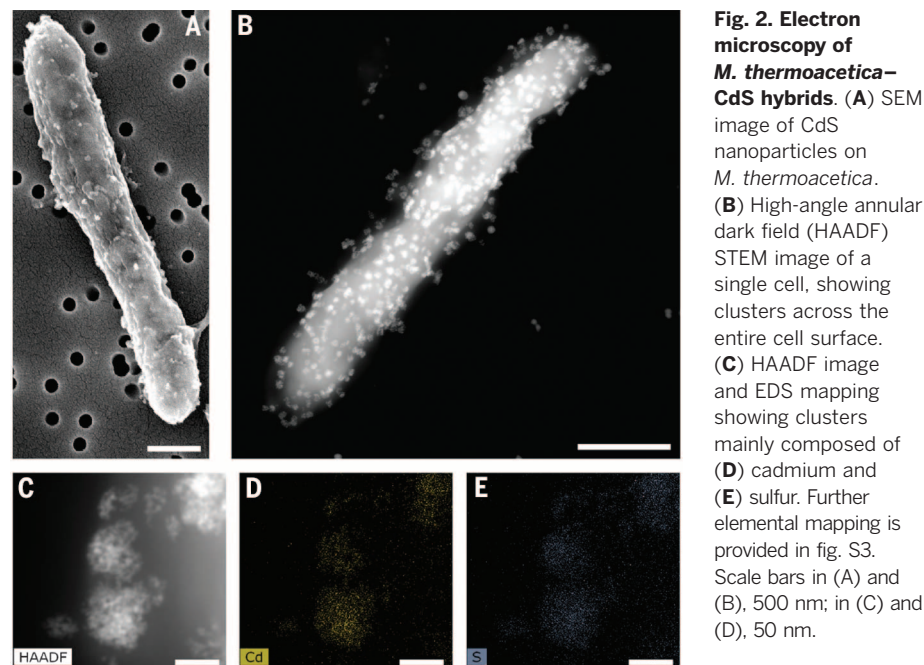
\*Corresponding author. E-mail: p\_yang@berkeley.edu



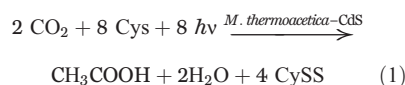
progressed (15), nonphotosynthetic bacteria remain the workhorse of synthetic biology, offering a facile way to tailor the product diversity from CO<sub>2</sub> reduction (16). Additionally, thermodynamic comparisons reveal substantial energetic advantages to photosensitizing nonphotosynthetic CO<sub>2</sub> reduction (17). Of particular interest is the Wood-Ljungdahl pathway, through which CO<sub>2</sub> is reduced to acetyl coenzyme A (acetyl-CoA), a common biosynthetic intermediate, and eventually to acetic acid, both of which can be further upgraded to high-value products by wild-type and genetically engineered organisms (10, 18). This pathway is also used by CO<sub>2</sub>-fixing electrotroths, enabling the use of semiconductor photoelectrons in this energetically efficient biosynthetic route.

We developed a hybrid system containing the nonphotosynthetic CO<sub>2</sub>-reducing bacterium *Moorella thermoacetica* (ATCC 39073) and its biologically precipitated CdS nanoparticles (19). CdS is a well-studied semiconductor with an appropriate band structure and is suitable for photosynthesis (20). As an acetogen and an electrothroph, *M. thermoacetica* serves as an ideal model organism to explore the capabilities of a hybrid system (21).

The photosynthesis of acetic acid by *M. thermoacetica* and CdS is a two-step, one-pot synthesis (Fig. 1). First, the precipitation of CdS by *M. thermoacetica* is triggered by the addition of Cd<sup>2+</sup> and cysteine (Cys) as the sulfur source (19, 22). *M. thermoacetica* uses photogenerated electrons from illuminated CdS nanoparticles to carry out photosynthesis (Fig. 1B). The absorption of a photon,  $h\nu$ , by CdS produces an electron and hole pair, e<sup>-</sup> and h<sup>+</sup>. The electron generates a reducing equivalent, [H] (see supplementary text and fig. S1 for elaboration of this process), that is passed on to the Wood-Ljungdahl pathway to synthesize acetic acid from CO<sub>2</sub>. Cysteine quenches the h<sup>+</sup>, leading to the oxidized disulfide form, cystine (CySS) (see supplementary text for the full set



of reaction equations). The overall photosynthetic reaction is



The precipitation of CdS by *M. thermoacetica* was initiated by the addition of Cd(NO<sub>3</sub>)<sub>2</sub> to an early exponential growth culture of glucose-grown cells supplemented with Cys (fig. S2) (19). Scanning electron microscopy (SEM), scanning transmission electron microscopy (STEM), and energy-dispersive x-ray spectroscopy (EDS) mapping revealed clusters of smaller nanoparticles (<10 nm;

Fig. 2, A and B) composed of cadmium and sulfur on the cells (Fig. 2, C to E, and fig. S3). Absorption spectra and Tauc plots yielded a measured direct band gap of  $2.51 \pm 0.05$  eV (fig. S4A). The slightly larger measured band gap relative to bulk CdS (2.42 eV) suggests the quantum confinement expected of <10-nm particles (20). Powder x-ray diffraction showed broad peaks consistent with small particles of the wurtzite phase (fig. S4B).

To confirm photosynthesis, a series of deletional control experiments was carried out in which *M. thermoacetica*, CdS, and light were systematically removed (Fig. 3, A and B). In the absence of light ( $405 \pm 5$  nm), acetic acid concentrations decreased [from ~2 mM accumulated under initial

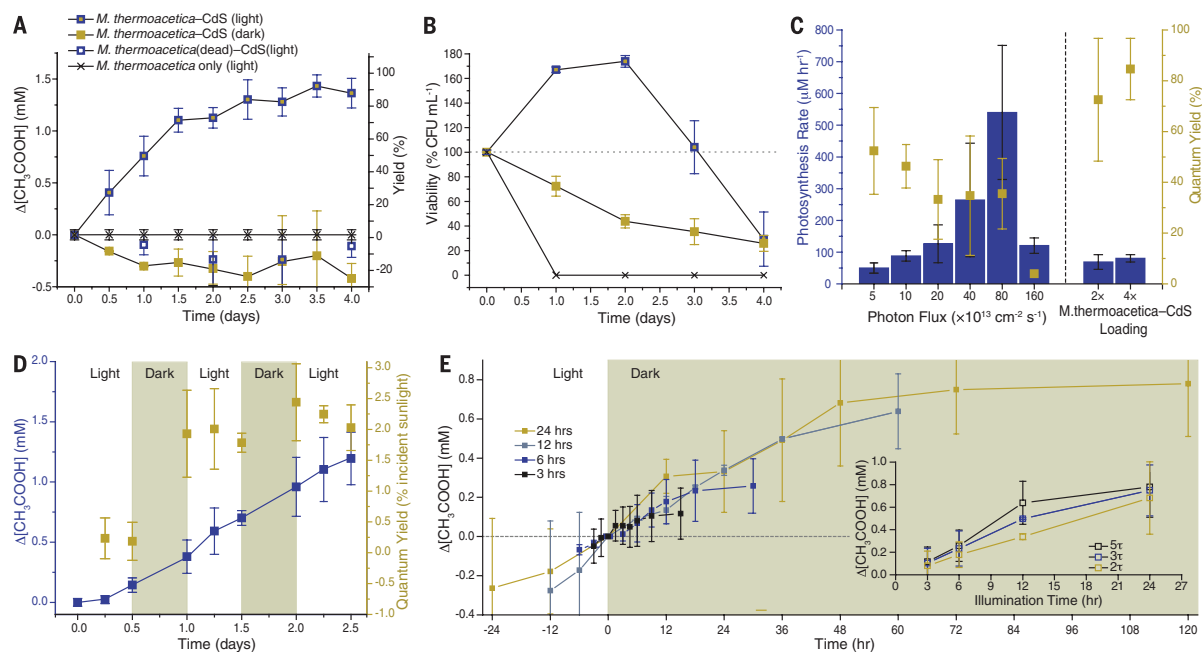


**Fig. 3. Photosynthesis behavior of *M. thermoacetica*-CdS hybrids.**

(A) Photosynthetic production of acetic acid by *M. thermoacetica*-CdS hybrids and deletional controls. The key applies to (A) and (B) only. (B) CFU viability assays for *M. thermoacetica*-CdS hybrids and deletional controls. (C) Rates of acetic acid production and quantum yields for increasing illumination intensities and *M. thermoacetica*-CdS concentrations. (D) Photosynthetic

acetic acid production under low-intensity simulated sunlight with light-dark cycles. (E) Acetic acid production under dark conditions for varying illumination times. The inset shows the relation between illumination time,  $\tau$ , and acetic acid yield under dark conditions at increasing multiples of  $\tau$ . All points and error bars show the mean and error-propagated SD, respectively, of triplicate experiments.

$\text{H}_2\text{CO}_2$  acclimation, as measured by quantitative proton nuclear magnetic resonance [ $^1\text{H}$ -qNMR spectroscopy], potentially as the result of a dark catabolic process. The viability determined by colony-forming units (CFU) assays slowly declined to  $\sim 25\%$  after 4 days (from the initial  $5.9 \pm 0.4 \times 10^4$  CFU  $\text{ml}^{-1}$  and  $1.7 \pm 0.4 \times 10^9$  cells  $\text{ml}^{-1}$ ), indicating that the *M. thermoacetica*-CdS system requires light to maintain viability. The viability of bare *M. thermoacetica* without CdS dropped to 0% within the first day under light, consistent with previous observations of semiconducting and/or insulating precipitates having a photoprotective role toward bacteria (23). Only *M. thermoacetica*-CdS hybrids exposed to light produced acetic acid. The  $^1\text{H}$ -qNMR spectrum revealed acetic acid to be the only product of  $\text{CO}_2$  reduction, confirming the high selectivity expected of biological catalysts (fig. S5). After the first 1.5 days, the rate of production began to plateau because of the limiting amounts of the sacrificial reductant, Cys.

We calculated a maximum yield of  $\sim 90\%$  acetic acid (based on the initial Cys concentration), which is consistent with previous observations that in the Wood-Ljungdahl pathway,  $\sim 10\%$  of reduced  $\text{CO}_2$  is directed toward cell biomass (24). During photosynthesis, both the viability and the cell counts of the *M. thermoacetica*-CdS system nearly doubled after the first day (fig. S6), on par with the doubling time of autotrophic growth ( $\sim 25$  hours). Although the growth was not vigorous and perhaps was limited by the total amount of CdS and other nutrients, these results suggest the possibility of a completely self-reproducing hybrid organism sustained purely through solar energy. After the

third and fourth days, viability decreased in coincidence with the depletion of Cys, leading to oxidative photodamage (fig. S7).

Under increasing blue light flux (435 to 485 nm), the rate of acetic acid production increased (Fig. 3C). At  $5 \times 10^{13}$  photons  $\text{cm}^{-2} \text{s}^{-1}$ , a quantum yield of  $52 \pm 17\%$  was observed. The rate of photosynthesis increased up to  $160 \times 10^{13}$  photons  $\text{cm}^{-2} \text{s}^{-1}$ , after which the rate dramatically decreased and the quantum yield dropped to  $4 \pm 1\%$ , possibly due to photooxidative degradation under high light intensities (25). At high light fluxes, large holes formed in the cell surface and, in some cases, resulted in the complete destruction of the cell membrane (fig. S7). The high quantum yield of the *M. thermoacetica*-CdS system is notable, given that previous analogous systems often have had reported quantum efficiencies of  $\sim 20\%$  (7). This result is rationalized by the low light flux of these measurements, which reduces losses from recombination (26). With four times the normal loading of *M. thermoacetica*-CdS hybrids, we measured a quantum yield of  $85 \pm 12\%$  (Fig. 3C). Under higher concentrations, the average flux per bacterium decreased, correlating with increased quantum yield.

To further characterize their photosynthetic behavior, we illuminated *M. thermoacetica*-CdS hybrids under low-intensity simulated sunlight (air mass 1.5 global spectrum,  $2 \text{ W m}^{-2}$ ) with a light-dark cycle of 12 hours each to mimic day-night cycles (Fig. 3D). Unexpectedly, acetic acid concentrations not only increased under illumination but continued to increase in the dark at the same rate, through several light-dark cycles.

A potential explanation lies in the accumulation of biosynthetic intermediates during the light cycle, which are then used during the dark cycle. These may include a number of reductive species [e.g., NADH (reduced nicotinamide adenine dinucleotide), NADPH (reduced NAD phosphate), or ferredoxin] or intermediates in the Wood-Ljungdahl pathway such as acetyl-CoA (27). A proton gradient may also be storing energy for adenosine triphosphate synthesis in the dark. Further experiments that varied the duration of the light cycle (Fig. 3E) revealed a proportionality between the length of illumination,  $\tau$ , and the acetic acid yield under dark conditions. Although the initial rate during and just after illumination appears to be relatively constant, consistent with a zero-order catalytic reaction, the yield begins to plateau after  $2\tau$ , exhibiting a linearity between illumination time and acetic acid yield (Fig. 3E, inset). However, at  $5\tau$ , samples that were illuminated for 24 hours break this trend. These observations suggest that during up to 12 hours of illumination, some intermediate accumulates, enabling a proportional acetic acid yield during the dark cycle. Beyond this, the intermediate may saturate, with longer illumination times yielding no further acetic acid. We measured a peak quantum yield of  $2.44 \pm 0.62\%$  of total incident low-intensity simulated sunlight (Fig. 3D). These quantum yields are order-of-magnitude comparable to the year-long averages determined for plants and algae, which range from  $\sim 0.2$  to  $1.6\%$  (7).

Biological routes to solid-state materials have often struggled to compete with high-quality traditionally synthesized materials. This work



demonstrates not only that biomaterials can be of sufficient quality to carry out useful photochemistry, but that in some ways they may be more advantageous in biological applications. Most traditional nanoparticle syntheses require organic capping ligands to control the particle shape. These ligands present a barrier to charge transfer between the semiconductor and the catalyst, often requiring electron tunneling (13). The ligand-free approach taken here may help to establish a favorable interface between the bacteria and the semiconductor, resulting in improved efficiencies. Additionally, metal chalcogenides such as CdS have had limited application because of oxidative photodegradation; the ability of bacteria to precipitate metal chalcogenides from the products of photodissolution (Cd<sup>2+</sup> and oxidized sulfur complex ions) suggests a potential regenerative pathway to circumvent the debilitating photoinstability through a precipitative self-regeneration.

The *M. thermoacetica*-CdS system displays behavior that may help it to exceed the utility of natural photosynthesis. First, the quantum yield increased with higher *M. thermoacetica*-CdS concentrations. The ability to tune the effective light flux per bacterium by changing the concentration of the suspension is a considerable advantage over similar light management practices in natural photosynthesis that are achieved through genetic engineering of chloroplast expression (28). Second, the catabolic energy loss observed during dark cycles in natural photosynthesis was absent in our hybrid system, which may be an innate feature of the Wood-Ljungdahl pathway, in which acetic acid is a waste product of normal respiration. Additionally, many plants and algae tend to store a large portion of their photosynthetic products as biomass, which requires extensive processing to produce useful chemicals. In contrast, the *M. thermoacetica*-CdS system directs ~90% of photosynthetic products toward acetic acid, reducing the cost of diversifying to other chemical products.

This system could be improved by substituting Cys oxidation with a more beneficial oxidation reaction, such as oxygen evolution, wastewater oxidation for water purification, or oxidative biomass conversion (29, 30). Expanding the material library available through biologically induced precipitation will increase the capacity for light absorption and raise the upper limit on semiconductor-bacteria photosynthetic efficiency. The availability of genetic engineering tools for *M. thermoacetica* (31), as well as the introduction of electrotrophic and nanoparticle precipitation behavior in model bacteria such as *Escherichia coli* (32, 33), suggests a potential role for synthetic biology in rationally designing such hybrid organisms.

Beyond the development of advanced solar-to-chemical synthesis platforms, this hybrid organism also has potential as a tool to study biological systems. The native integration of semiconductor nanoparticles with bacterial metabolic processes provides a distinctive optical tag for the study of microbial behavior, such as semiconductor-bacteria electron transfer (34, 35), by providing a sensitive, noninvasive, nonchemical probe.

## REFERENCES AND NOTES

1. A. W. D. Larkum, *Curr. Opin. Biotechnol.* **21**, 271–276 (2010).
2. D. Gust, T. A. Moore, A. L. Moore, *Acc. Chem. Res.* **42**, 1890–1898 (2009).
3. R. E. Blankenship *et al.*, *Science* **332**, 805–809 (2011).
4. T. J. Meyer, *Acc. Chem. Res.* **22**, 163–170 (1989).
5. A. M. Appel *et al.*, *Chem. Rev.* **113**, 6621–6658 (2013).
6. A. S. Hawkins, P. M. McTernan, H. Lian, R. M. Kelly, M. W. W. Adams, *Curr. Opin. Biotechnol.* **24**, 376–384 (2013).
7. K. A. Brown, M. B. Wilker, M. Boehm, G. Dukovic, P. W. King, *J. Am. Chem. Soc.* **134**, 5627–5636 (2012).
8. J. P. Giraldo *et al.*, *Nat. Mater.* **13**, 400–408 (2014).
9. J. P. Torella *et al.*, *Proc. Natl. Acad. Sci. U.S.A.* **112**, 2337–2342 (2015).
10. C. Liu *et al.*, *Nano Lett.* **15**, 3634–3639 (2015).
11. L. Lapinonnière, M. Picot, F. Barrière, *ChemSusChem* **5**, 995–1005 (2012).
12. K. P. Nevin *et al.*, *Appl. Environ. Microbiol.* **77**, 2882–2886 (2011).
13. P. W. King, *Biochim. Biophys. Acta* **1827**, 949–957 (2013).
14. W. J. Crookes-Goodson, J. M. Slocik, R. R. Naik, *Chem. Soc. Rev.* **37**, 2403–2412 (2008).
15. D. C. Ducat, P. A. Silver, *Curr. Opin. Chem. Biol.* **16**, 337–344 (2012).
16. L. S. Gronenberg, R. J. Marcheschi, J. C. Liao, *Curr. Opin. Chem. Biol.* **17**, 462–471 (2013).
17. A. G. Fast, E. T. Papoutsakis, *Curr. Opin. Chem. Eng.* **1**, 380–395 (2012).
18. M. C. A. Van Eerten-Jansen *et al.*, *ACS Sustainable Chem. Eng.* **1**, 513–518 (2013).
19. Materials and methods are available as supplementary materials on Science Online.
20. R. Vogel, P. Hoyer, H. Weller, *J. Phys. Chem.* **98**, 3183–3188 (1994).
21. H. L. Drake, S. L. Daniel, *Res. Microbiol.* **155**, 869–883 (2004).
22. D. P. Cunningham, L. L. Lundie Jr., *Appl. Environ. Microbiol.* **59**, 7–14 (1993).
23. J. D. Holmes *et al.*, *Photochem. Photobiol.* **62**, 1022–1026 (1995).
24. S. L. Daniel, T. Hsu, S. I. Dean, H. L. Drake, *J. Bacteriol.* **172**, 4464–4471 (1990).
25. E. Dumas *et al.*, *Environ. Sci. Technol.* **44**, 1464–1470 (2010).
26. B. Liu, X. Zhao, C. Terashima, A. Fujishima, K. Nakata, *Phys. Chem. Chem. Phys.* **16**, 8751–8760 (2014).
27. K. Schuchmann, V. Müller, *Nat. Rev. Microbiol.* **12**, 809–821 (2014).
28. B. Hankamer *et al.*, *Physiol. Plant.* **131**, 10–21 (2007).
29. H. G. Cha, K.-S. Choi, *Nat. Chem.* **7**, 328–333 (2015).
30. B. E. Logan, K. Rabaey, *Science* **337**, 686–690 (2012).
31. A. Kita *et al.*, *J. Biosci. Bioeng.* **115**, 347–352 (2013).
32. H. M. Jensen *et al.*, *Proc. Natl. Acad. Sci. U.S.A.* **107**, 19213–19218 (2010).
33. C. L. Wang, A. M. Lum, S. C. Ozuna, D. S. Clark, J. D. Keasling, *Appl. Microbiol. Biotechnol.* **56**, 425–430 (2001).
34. M. Rosenbaum, F. Aulenta, M. Villano, L. T. Angenent, *Bioresour. Technol.* **102**, 324–333 (2011).
35. J. S. Deutzmann, M. Sahin, A. M. Spormann, *mBio* **6**, e00496-15 (2015).

## ACKNOWLEDGMENTS

The interface design part of this work was supported by the U.S. Department of Energy under contract no. DE-AC02-05CH11231 (PChem). Work at the Molecular Foundry was supported by the Office of Science, Office of Basic Energy Sciences, of the U.S. Department of Energy under contract no. DE-AC02-05CH11231. Solar-to-chemical production experiments were supported by NSF (grant DMR-1507914). The authors thank J. J. Gallagher and M. C. Y. Chang for the original inoculum of *M. thermoacetica* ATCC 39073. K.K.S. acknowledges support from the NSF Graduate Research Fellowship Program under grant DGE-1106400. The authors thank the National Center for Electron Microscopy. All data are available in the body of the paper or in the supplementary materials.

## SUPPLEMENTARY MATERIALS

www.sciencemag.org/content/351/6268/74/suppl/DC1  
Materials and Methods  
Supplementary Text  
Figs. S1 to S9

28 August 2015; accepted 19 November 2015  
10.1126/science.aad3317

## VIROLOGY

## An orthopoxvirus-based vaccine reduces virus excretion after MERS-CoV infection in dromedary camels

Bart L. Haagmans,<sup>1\*</sup> Judith M. A. van den Brand,<sup>1</sup> V. Stalin Raj,<sup>1</sup> Asisa Volz,<sup>2</sup> Peter Wohlsein,<sup>3</sup> Saskia L. Smits,<sup>1</sup> Debby Schipper,<sup>1</sup> Theo M. Bestebroer,<sup>1</sup> Nisreen Okba,<sup>1</sup> Robert Fux,<sup>2</sup> Albert Bensaid,<sup>4</sup> David Solanes Foz,<sup>4</sup> Thijs Kuiken,<sup>1</sup> Wolfgang Baumgärtner,<sup>3</sup> Joaquim Segalés,<sup>5,6</sup> Gerd Sutter,<sup>2\*</sup> Albert D. M. E. Osterhaus<sup>1,7,8\*</sup>

Middle East respiratory syndrome coronavirus (MERS-CoV) infections have led to an ongoing outbreak in humans, which was fueled by multiple zoonotic MERS-CoV introductions from dromedary camels. In addition to the implementation of hygiene measures to limit further camel-to-human and human-to-human transmissions, vaccine-mediated reduction of MERS-CoV spread from the animal reservoir may be envisaged. Here we show that a modified vaccinia virus Ankara (MVA) vaccine expressing the MERS-CoV spike protein confers mucosal immunity in dromedary camels. Compared with results for control animals, we observed a significant reduction of excreted infectious virus and viral RNA transcripts in vaccinated animals upon MERS-CoV challenge. Protection correlated with the presence of serum neutralizing antibodies to MERS-CoV. Induction of MVA-specific antibodies that cross-neutralize camelpox virus would also provide protection against camelpox.

**C**oronaviruses (CoVs) cause common colds in humans, but zoonotic transmissions occasionally introduce more pathogenic viruses into the human population. For example, the SARS-CoV caused the 2003 outbreak of severe acute respiratory syndrome (SARS). In 2012,

a previously unknown virus, now named Middle East respiratory syndrome CoV (MERS-CoV), was isolated from the sputum of a 60-year-old Saudi Arabian man who suffered from acute pneumonia and subsequently died (1, 2). Several infection clusters have been reported over the past